Layered Quaternary Compounds in the Cu 2 S–In 2 S 3 –Ga 2 S 3 system

Maria Teresa Caldes, Eric Gau- Tron, Maria Teresa Caldes, Catherine Guillot-Deudon, Angelica Thomere, Margaux Penicaud, Eric Gautron, Philippe Boullay, Martine Bujoli-Doeuff, Nicolas Barreau, et al.

Layered quaternary compounds in the Cu_2S-In_2S_3-Ga_2S_3 system

Maria Teresa Caldes*, Catherine Guillot-Deudon*, Angelica Thomere, Margaux Penicaud, Eric Gautron, Philippe Boullay†, Martine Bujoli-Doeuff, Nicolas Barreau, Stéphane Jobic, Alain Lafond

Institut des Matériaux Jean Rouxel – Université de Nantes, CNRS, 2 rue de la Houssinière, BP 32229, 44322 Nantes Cedex 3, France

†CRISMAT, CNRS, Normandie University, ENSICAEN, UNICAEN, 14000 Caen, France

ABSTRACT: Several new materials, $Cu_{0.32}In_{1.74}Ga_{0.84}S_4$ ($CIGS_4$), $Cu_{0.65}In_{1.75}Ga_{1.4}S_5$ ($CIGS_5$), $Cu_{1.44}In_{2.77}Ga_{0.76}S_6$ ($CIGS_6$) and $Cu_{1.1}In_{2.49}Ga_{1.8}S_7$ ($CIGS_7$) have been evidenced in the Cu_2S-In_2S_3-Ga_2S_3 pseudo ternary system. All of them present a 2D structure built upon infinite $2/\infty[InS_2]$ layers ((InS_6) octahedra sharing edges) on which condense on both side mono-, bi-, or tri-$2/\infty[MS]$ layers ((MS_4) tetrahedra (M = Cu, In, Ga) sharing corners). $(M(Td))_{n-2}(In(Oh))S_n$ slabs are separated from each other by a van der Waals gap and subscript n refers to the number of sulfur layers within the building block. These compounds have the propensity to display stacking faults but also polymorphic forms. Their optical gap (ca. 1.7 eV) is quite similar to the one of the $Cu(In_{0.7}Ga_{0.3})S_2$ chalcopyrite absorbers used in tandem solar cells, and the major charge carriers are holes. This suggests that they might be very attractive for photovoltaic applications in thin film devices but also for photocatalysis.

KEYWORDS : layered CIGS sulfides, crystal structure, electron crystallography, HAADF-imaging, XPS, photovoltaics.

1.Introduction

Among the different photovoltaic technologies, thin film solar cells using a chalcogenide as absorber still awakens interest. Namely, in that context, the quaternary $Cu(In,Ga)Se_2$ (CIGSe) p-type semiconductor has been extensively studied. Beyond its ability to absorb impinging light and the right position in energy of its valence and conduction bands, one major advantage of this material resides in the ability of its chalcopyrite structure to accommodate a large off-stoichiometry. This makes possible to adjust the chemical composition to desired physical characteristics. In the specific case of CIGSe, it is very well know that a copper deficient (Cu-poor CIGSe) could play a key role for optimizing performances of the cells [1]. Nowadays, the homologous sulfide compound received much less attention even if investigations have been carrying out for potential applications in tandem solar cells.

Therefore, we studied the $Cu_{1-z}(In_{1-x}Ga_x)_{1+z/3}S_2$ series (Cu-poor CIGS) and an extended pseudo ternary phase diagram Cu_2S-In_2S_3-Ga_2S_3 for the compositions $0.2 \leq x \leq 1$ and $0 \leq z \leq 0.6$ could be established [2]. Noticeably, it was clearly demonstrated that the chalcopyrite structure is much less tolerant towards the copper deficiency in sulfides than in selenides, probably in relation with a lesser covalent character of the cation-anion bonding. A small copper deficiency ($z > 0.1$) is enough to induce a total collapse of the 3D atomic packing of the chalcopyrite edifice in CIGS, while such a collapse has never been evidenced in CIGSe. This deviation to the ideal stoichiometry triggers the formation of quaternary CIGS layered compounds.

Since copper deficient phases play a determining role on the performance of solar cells, it seemed important to prepare these new compounds as single phases in order to evaluate their optoelectronic properties before their possible deposition as thin films for solar cells.

In this work, four new layered quaternary compounds in Cu_2S-In_2S_3-Ga_2S_3 system have then been identified by combining single-crystal X-ray diffraction, electron diffraction and chemical analysis by EDX. Three of them were successfully prepared as single-phases. Their optical band gaps were then evaluated by diffuse reflectance and the relative valence band maximum (VBM) positioning was determined by XPS.

2. Experimental Section

2.1 Synthesis

Single crystals were issued from three members of the $Cu_{1-z}(In_{1-x}Ga_x)_{1+z/3}S_2$ series: $Cu_{0.4}(In_{0.5}Ga_{0.5})_{1.2}S_2$ (z=0.6, x=0.5), $Cu_{0.4}(In_{0.7}Ga_{0.3})_{1.2}S_2$ (z=0.6, x=0.3) and $Cu_{0.7}(In_{0.7}Ga_{03})_{1.1}S_2$ (z=0.3, x=0.3). These compounds were prepared by solid state reactions at high temperature from elemental precursors (Cu,

Alfa Aesar 99.9%; In, In corp. of America 6N, Ga, Alfa Aesar-pellet 6mm diam. 6N and S, Aldrich, 99.998%) weighted in stoichiometric ratios. After grinding, the mixture was heated at 100°C/h in a quartz ampoule sealed in vacuum up to 850°C for 96h or 170h or more depending on the samples, and then cooled down to room temperature either by quenching or by cooling at 100°C/h. One or more annealing in the same conditions were sometimes required to homogenize the materials. Sulfurization synthesis under H_2S was occasionally used. A mixture of CuO (Aldrich, 99.99%), In_2O_3 (Alfa Aesar, 99.995%) and Ga_2O_3 (Alfa Aesar, 99.999%) was heated at 900°C during 3h. A posterior heat treatment at 850°C for 170h was done in a quartz ampoule sealed in vacuum. The synthesis conditions for each of the targeted compositions prepared are summarized in Table S1.

Thin films were prepared by the coevaporation of the elements in high vacuum from effusion cells (copper, indium, gallium and sulfur) using so-called one-step process. After the deposition, the thin films were dipped in a KCN solution (0.1M for 5 min) to remove Cu_xS_y from the surface. The average composition was determined by EDX analysis.

2.2 Chemical analyses

The chemical compositions of the prepared samples were analyzed using an EDX-equipped scanning electron microscope (JEOL 5800LV) on polished sections of the products embedded in epoxy. The elemental percentages were calculated using calibrated internal standards under the following operating conditions: accelerating voltage 20 kV, standards Cu (Cu Kα), In (InAs Lα), Ga (GaP K) and S (FeS_2 Kα). This technique allowed us also to check the chemical homogeneity of samples.

2.3 Powder X-ray diffraction

The powder X-ray diffraction (PXRD) experiments were performed with the use of a Bruker D8 Advance diffractometer (Bragg Brentano, θ/2θ geometry, CuK-L3, λ = 1.540598 Å) equipped with a LynxEye detector. All the powder patterns were recorded in the 4°- 100° 2θ- range with a 2θ-step of 0.011°. Le Bail and Rietveld analyses were carried out with the help of the program JANA2006 [3].

2.4 Single crystal X-ray diffraction.

Suitable single crystals were picked up in each of powdered samples. The studied crystals were often of poor quality because of their lamellar feature (see below). The data collections were carried out at ambient temperature on a Bruker-Nonius Kappa CCD diffractometer using graphite monochromatic MoKα. Data integration was processed with the set of programs from Nonius using the Eval CCD formalism. The crystal shape and size optimization for absorption were performed with the X-Shape program while refinements were carried out with the JANA2006 program.

2.5 Transmission electron microscopy

High-angle annular dark-field imaging (HAADF) was performed with a probe corrected scanning transmission electron microscope (S/TEM) Themis-Z (Thermo Fisher Scientific) with these experimental conditions: 300 kV accelerating voltage, 21 mrad convergence angle, 63-200 mrad collection angle. The compounds were gently ground in ethanol before being deposited on a holed carbon film supported by a copper grid for examination. Precession electron diffraction tomography (PEDT), was performed with a Jeol 2010 electron microscope (operating at 200 kV with a LaB6 cathode) equipped with a Nanomegas DigiStar precession module and an upper-mounted Gatan ORIUS 200D CCD camera. PEDT data sets of nonoriented patterns were recorded on several different thin crystals. For data collections the precession angle was set to 1.6° with a goniometer tilt step 1°. PEDT data sets were analyzed using the computer programs PETS [4] and JANA2006.

2.6 X-ray photoelectron spectroscopy

X-ray photoelectron spectroscopy (XPS) measurements were performed on a Kratos axis Nova spectrometer (monochromatic Al Kα X-ray source, 1486.6 eV). Studies were carried out on pellets mounted on double-sided carbon tape on an alumina plate. An electron flood gun was used to eliminate any surface charging effect. The pass energy was 160 eV for wide scan spectra and 40 eV for narrow scan and the valence band (VB) region (instrumental resolution of 0.1 eV). Spectra were calibrated using the C 1s peak at 284.8 eV. All high-resolution spectra were analyzed and fitted with the CasaXPS software [5]. The valence band maximum (VBM) position was determined for all probed samples by linearly extrapolating the low binding energy (BE) edge of the VB region

2.7 Diffuse reflectance measurements

The ultraviolet–visible light–near-infrared (UV-vis-NIR) diffuse reflectance spectra of finely ground samples were recorded with a UV/vis/NIR spectrometer (PerkinElmer Lambda 1050) equipped with an integration sphere. The UV Winlab 6 program was used to control experiments. The reflectance measurements were made in the 850–400 nm range (i.e. 1.46 eV- 3.10 eV) at a resolution of 2 nm. A barium carbonate blank was used to normalize the measured reflectance. The absorption (K/S) data were then calculated from the raw reflectance using the $K/S = (1 R)^2/(2R)$ Kubelka-Munk function [6]. The optical gap value was determined for all probed samples by linearly extrapolating.

3. Results and discussion

As already mentioned by Thomere et al., attempts to synthesize $Cu_{1-z}(In_{1-x}Ga_x)_{1+z/3}S_2$ compounds [2] systematically leads to multiphasic samples for z> 0.1 (see pseudo-ternary diagram shown in Figure 1). Typical PXRD patterns corresponding to nominal compositions $Cu_{0.7}(In_{0.7}Ga_{03})_{1.1}S_2$ (z=0.3, x=0.3), $Cu_{0.4}(In_{0.7}Ga_{0.3})_{1.2}S_2$ (z=0.6, x=0.3) and $Cu_{0.4}(In_{0.5}Ga_{0.5})_{1.2}S_2$ (z=0.6, x=0.5) are shown in Figure S 1. Corresponding targets are imaged in Figure 1.

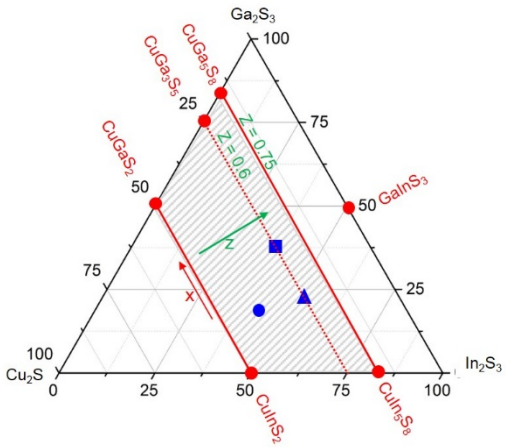

Figure 1. Pseudo-ternary diagram of the Cu_2S-In_2S_3-Ga_2S_3 system. x refers to the Ga/(Ga+In) ratio, and z to the copper deficiencies relative to the Cu(In,Ga)S_2 composition The hashed zone corresponds to a multiphasic domain. Following targeted compositions are imaged as blue symbols: $Cu_{0.4}(In_{0.5}Ga_{0.5})_{1.2}S_2$ (square), $Cu_{0.4}(In_{0.7}Ga_{0.3})_{1.2}S_2$ (triangle) and $Cu_{0.7}(In_{0.7}Ga_{03})_{1.1}S_2$ (circle)

As inferred from the d-spacing values observed at low two-theta angles (i.e. 12 Å, 15.7 Å, 18.7 Å and 21.7 Å), several new quaternary phases, very Cu-poor compared to Cu($In_{1-x}Ga_x$)S_2 chalcopyrite (SG $I\bar{4}2d$, a~5.47 Å, c~10.96 Å), were identified (see Table 1). This fact was exemplified in Figure 2 where three of the four phases identified, were detected by combining XRD, electron diffraction and backscattered electron imaging analysis. Each of the first three reflections observed in the DRX pattern, corresponds respectively to the inter-reticular distance d (001) of each new phase. The fourth one has been detected in the targeted composition $Cu_{0.4}(In_{0.7}Ga_{0.3})_{1.2}S_2$ (see Figure S1).

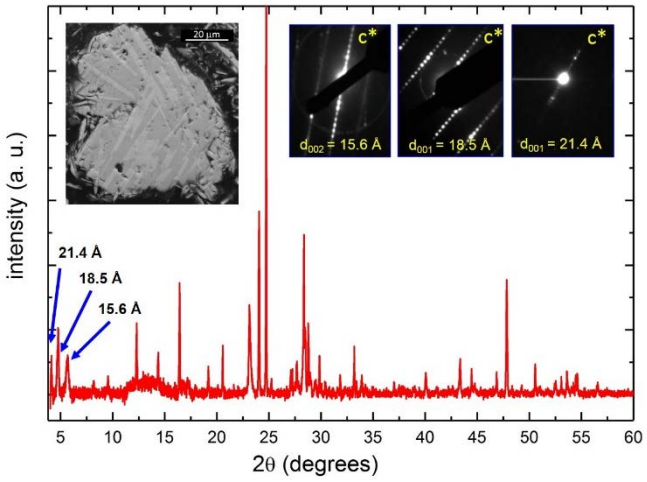

Figure 2. XRD pattern of $Cu_{0.4}(In_{0.5}Ga_{0.5})_{1.2}S_2$ multiphasic compound. ED patterns corresponding to three different phases are shown at top right of the image. In the top left, the SEM backscattered electron image evidences the coexistence several phases.

Some of these d-spacing have already been described for some layered compounds in the Ga_2S_3-In_2S_3 system: $GaInS_3$ (c=18.2 Å) [7], $Ga_{0,75}In_{1,25}S_4$ (c=12.23 Å) [8], $Ga_{1,74}In_{2,92}S_7$ (c=21.14 Å) [9]. However, they have never been reported before for quaternary compounds in the pseudo-ternary diagram Cu_2S-In_2S_3-Ga_2S_3. Moreover, the structural models proposed for $Ga_{0,75}In_{1,25}S_4$ (c=12.23 Å) and $Ga_{1,74}In_{2,92}S_7$ (c=21.14 Å) do not respect the criteria of charges neutrality:

In Table 1 the multiphase feature of three targeted compositions is illustrated. Four different Cu/S ratios are thus identified: one corresponding to the chalcopyrite structure (Cu/S = 0.49) and three others corresponding to new quaternary Cu-poor phases. The In/S and Ga/S ratios can be different for the same Cu/S ratio."

Table 1. EDX atomic ratios of quaternary phases detected in each multiphasic sample. The different colors figure out dissimilar Cu/S ratios.

Targeted composition		Cu/S	In/S	Ga/S
$Cu_{0.4}(In_{0.5}Ga_{0.5})_{1.2}S_2$	phase 1	0.27(3)	0.14(2)	0.50(3)
	phase 2	0.19(2)	0.28(3)	0.39(3)
	phase 3	0.18(2)	0.34(3)	0.30(3)
$Cu_{0.7}(In_{0.7}Ga_{0.3})_{1.1}S_2$	chalco-pyrite	0.49(3)	0.30(3)	0.23(2)
	phase 2	0.27(3)	0.43(3)	0.16(2)
$Cu_{0.4}(In_{0.7}Ga_{0.3})_{1.2}S_2$	phase 1	0.19(2)	0.43(3)	0.19(2)
	phase 2	0.08(2)	0.44(3)	0.23(2)

To solve the structure of these new quaternary compounds, four suitable crystals were picked up in the three aforementioned powdered samples. Their chemical composition was obtained by EDX analyses.

Clearly, four types of layered compounds were identified. They were named $CIGS_4$ ($Cu_{0.32}In_{1.74}Ga_{0.84}S_4$), $CIGS_5$ ($Cu_{0.65}In_{1.75}Ga_{1.4}S_5$), $CIGS_6$ ($Cu_{1.44}In_{2.77}Ga_{0.76}S_6$) and $CIGS_7$ ($Cu_{1.1}In_{2.49}Ga_{1.8}S_7$), according to both chemical composition and number of anionic layers in the structure (i.e. S_n).

The structures of $CIGS_4$-CGS_7 are depicted in Figure 3. All exhibit a marked 2D character with $2/\infty[InS_2]$ layers built upon (InS_6) octahedra sharing edges (CdI-like slabs) on which condense on both side mono-, bi-, or tri- $2/\infty[MS]$ layers that consist of (MS_4) tetrahedra (M = Cu, In, Ga) sharing corner. This leads to $(M_{(Td)})_{n-2}(In_{(Oh)})S_n$ slabs separated to each other by a van der Waals gap of about 3.75 Å. $CIGS_n$ phases are consequently characterized by specific d-spacing, ca. 12.2, 15.7, 18.7 and 21.7 Å for $CIGS_4$, $CIGS_5$, $CIGS_6$ and $CIGS_7$, related to their slabs thickness. Let us notice that n can be even or odd. In the latter case, this implies that the number of MS layers above a $2/\infty[InS_2]$ layer is different from the number of MS layers below (and vice versa) with distribution of Cu, In and Ga atoms on Td sites possibly distinct above and below.

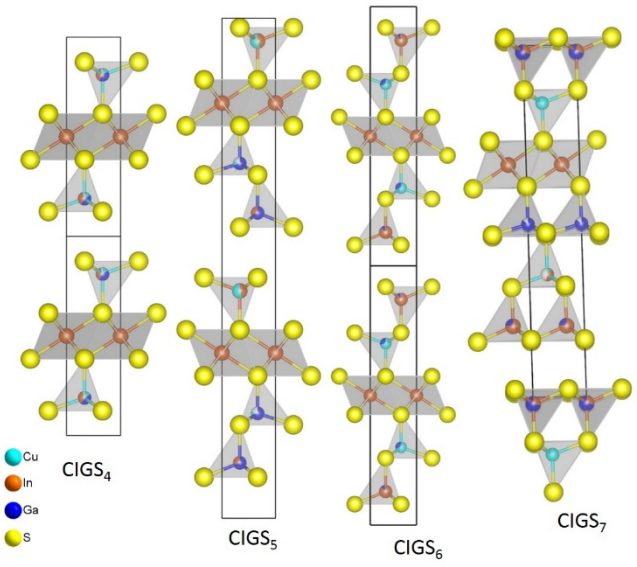

Figure 3. Structure models of $CIGS_4$ ($Cu_{0.32}In_{1.74}Ga_{0.84}S_4$), $CIGS_5$ ($Cu_{0.65}In_{1.75}Ga_{1.4}S_5$), $CIGS_6$ ($Cu_{1.44}In_{2.77}Ga_{0.76}S_6$) and $CIGS_7$ ($Cu_{1.1}In_{2.49}Ga_{1.8}S_7$).

Refinement results for all compounds are given in Table 2. All the structures were refined in P63*mc* space group or its subgroup P-3*m*1. Atomic positions and atomic displacements parameters (ADP) are shown in Tables S2-S5.

Table 2. Main crystal data and structure refinement results for $CIGS_n$ phases

	$CIGS_4$	$CIGS_5$	$CIGS_6$	$CIGS_7$
a (Å) [2]	3.8203(6)	3.7898(2)	3.8506(2)	3.7933(3)
c (Å) [2]	12.182(2)	30.664(3)	18.704(2)	21.540(14)
S G	P-3*m*1	P63*mc*	P-3*m*1	P 3*m*1
N_{obs}/N_{all}	2012/2348	8291/8990	5212/5762	1617/2788
R_{int}(obs/all)	5.83/6.07	5.86/5.88	4.41/4.46	17.41/22.74
# ref. par.	13	28	19	39
N_{obs}/N_{all}	263/313	725/764	455/487	469/801
R(obs/all)	6.12/7.04	5.15/5.34	6.70/7.03	11.84/21.48
R_w(obs/all)	21.38/21.60	14.48/14.56	22.34/22.43	19.01/22.31
ρ (e^-/Å^3)+/-	6.38/-3.08	3.32/-2.69	5.21/-3.73	10.58/-7.33

For all crystals, the octahedral sites (Oh) are exclusively and fully occupied by indium atoms. In contrast, tetrahedral sites (Td) can be partially vacant and a mixed occupancy is often observed. Because Cu^+ and Ga^{3+} cations are isoelectronic and not distinguishable by conventional X-ray diffraction, the occupation of mixed Td sites was determined by considering simultaneously various criteria, namely the chemical composition of the single crystals revealed by EDX, the evolution of the ADPs during the refinement, and the value of the cation-sulfur distances refined for each type of site. Interatomic distances for the four refined compounds $CIGS_4$, $CIGS_5$, $CIGS_6$ $CIGS_7$ are gathered in Table S6. They all match with those reported in the literature for other phases with similar chemical environments [10–12]. As expected, the In-S bond distances in a octahedral site (2.6 Å, $r_{In}^{3+}(Oh)$ = 0.80 Å) are larger than the In-S bonds in tetrahedral environment (~2.4 Å, $r_{In}^{3+}(Td)$ = 0.60 Å) that are larger than Cu(Ga)-S ones (~2.3 Å, $r_{Cu}^{+}(Td)$ = 0.46 Å, $r_{Ga}^{3+}(Td)$ = 0.47 Å). However, the presence of vacancies leads systematically to a slight shortening of cation-sulfur bond distances compared to the expected ones. In these lamellar compounds, the vacancy rate of Td sites never exceeds 20% except for $CIGS_7$ in which a mixed site (In-Cu) exhibits a vacancy rate of 50%. It is also worth noticing that indium atoms in tetrahedral sites are preferentially located at the van de Waals gap frontier, probably for steric reasons

Indeed, $CIGS_4$ with a sequence $Td_{(Cu,In,Ga,□)}$-$Oh_{(In)}$-$Td_{(Cu,In,Ga,□)}$ sequence, $CIGS_5$ ($Td_{(In,Ga)}$-$Td_{(Cu,Ga,□)}$-$Oh_{(In)}$-$Td_{(Cu,In)}$) and $CIGS_6$ ($Td_{(Cu,Ga)}$-$Td_{(Ga,In,□)}$-$Oh_{(In)}$-$Td_{(Cu,Ga)}$-$Td_{(Ga,In,□)}$) are isostructural to $ZnIn_2S_4$-type I, $Zn_2In_2S_5$-type IIa and $Zn_3In_2S_6$, respectively [13]. The $CIGS_5$ stacking type has been also already observed for $Ag_{1.25}Ga_{2.5}In_{3.75}S_{10}$ [14]. Conversely $CIGS_7$ ($Td_{(In,Ga)}$-$Td_{(Cu,In,□)}$-$Td_{(Ga,□)}$-$Oh_{(In)}$-$Td_{(In,Ga)}$-$Td_{(Cu)}$) exhibits an unprecedented layered stacking. At this stage, let us also mention that $GaInS_3$ [7], $Ga_{0.75}In_{1.25}S_4$ (c=12.23 Å) [8], $Ga_{1.74}In_{2.92}S_7$ (c=21.14 Å) [9] are probably also members of the aforementioned series (n= 6, n= 4 and n=7, respectively) but for two last compounds, a chemical element is obviously missing to respect the charge balance.

Although we have been able to elucidate the structure of these four quaternary phases using X-ray single crystal diffraction, it is worth noting that the R_w remain high for all the structures and Fourier difference maps show large residuals along c axis. The high values of R_w are partially due to the difficulty to describe accurately the occupation of Td sites, since the intensity of several strong reflections highly depends on it**.** On the other hand, the faulted feature of the crystals can also lead to large errors. Due to the strong structural similarity in between $(M_{(Td)})_{n-2}In_{(Oh)}$ S_n blocks and the 2D character of these building entities, intergrowths, stacking faults and turbostratic disorder could exist that may explain difficulties met to properly refine structures. In fact, the quality of the single crystals was often poor. To illustrate this purpose, the experimental (hol) * reciprocal plane corresponding to the single crystal of $CIGS_4$ is shown in figure S2. The extra reflections observed along the c* axis, could be attributed to the stack of several platelets (see

inserted image) but probably also to the existence of stacking faults. Although these extra reflections are not considered during integration process, their presence could induce an error during intensities measurement. For all these reasons, the structure models of $CIGS_n$ should probably be considered as average structures.

In Figure 4, the [100] electron diffraction pattern of a faulted crystal and its corresponding TEM image are shown. The streaking of diffraction spots observed along c*-axis testify of a strong structural disorder. Actually, the Z-contrast image (HAADF-STEM) figures out intergrowths. In this type of images, the brightness level is proportional to the averaged atomic number of the projected atomic columns observed. Accordingly, the $2/\infty$ $[InS_2]$ octahedral layers appear as brighter spots rows and tetrahedral (MS_4) ones like gray rows. The Van der Waals gap is imaged as a dark area. The number of tetrahedral layers on each side of the $2/\infty$ $[InS_2]$ layers can be then easily counted and the different members of the series $(M_{(Td)})_{n-2}(In_{(Oh)})S_n$ can thus be identified (see annotations in Figure 4 and Figure S2 for a large field of view).

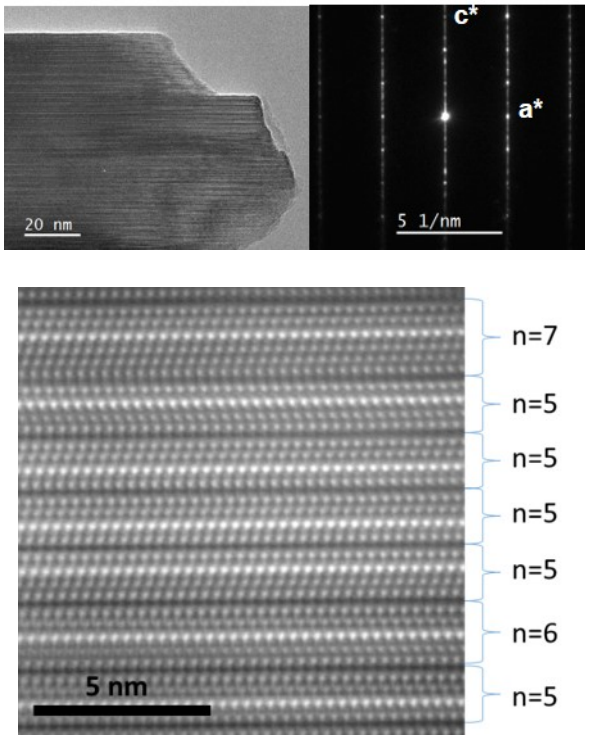

Figure 4. [100] electron diffraction pattern, corresponding TEM image and HAADF-STEM image (on the bottom) of a faulted crystal, highlighting the propensity of $CIGS_n$ materials to contain intergrowth defects (the value n from $(M_{(Td)})_{n-2}(In_{(Oh)})S_n$ is given for each slab). The van der Waals gaps are imaged as dark contrast lines.

Therefore, we decided to reduce the size of the probe, in order to find nanocrystals much better organized than those used for SCXRD. Thus, we investigated the structure of $CIGS_n$ phases using PEDT. Faulted crystals were also evidenced irrespective of their size. Nonetheless, it was possible to solve the 2Td-Oh-2Td layer stacking of $CIGS_6$ and refined it [15] to a final model consistent with that obtained by SCXRD. Taking into account the charge balance equilibrium and thermal displacement parameters, the final refinement led to the following chemical formula $Cu_{1.2}In_{2.54}Ga_{1.06}S_6$. Refinements results are summarized in Tables S7-S8. The chemical composition of the crystal studied by PEDT is significantly different from that of one studied by SCDRX ($Cu_{1.44}In_{2.77}Ga_{0.76}S_6$). This feature is possible due to the great occupation flexibility (Cu, Ga, In) exhibited by Td-sites in these lamellar structures. Indeed, for a given $CIGS_n$ structure-type, different chemical compositions may exist.

To try to obtain $CIGS_n$ compounds as powdered single-phase samples, prior synthesis conditions were modified Instead of using elements as reactants, gallium, indium and copper sulphides were used. On the other hand, the reaction time was reduced from 170 to 48 hours and samples were quenched. Chemical compositions of single crystals studied were used as target. Figure S3 and Figure 5 display the PXRD patterns of as-prepared $CIGS_4$, $CIGS_5$ and $CIGS_6$ compounds (attempts to prepare $CIGS_7$ as powder without sub-products in large amount never succeeded).

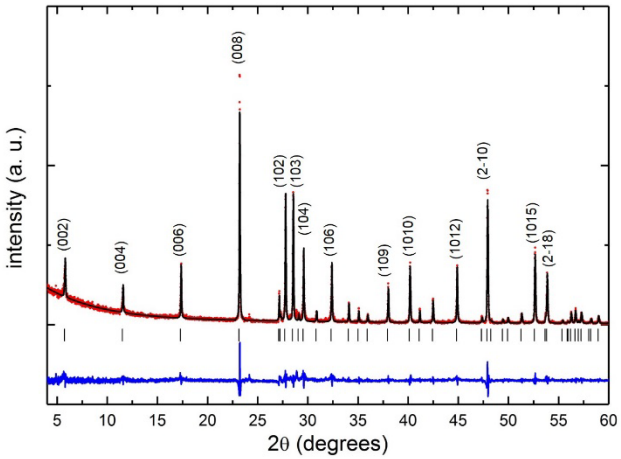

Figure 5. XRD pattern and Le Bail refinement of $CIGS_5$ compound

For all compounds, Le Bail refinements attest that most of the observed reflections can be indexed considering unit cells parameters and space groups obtained by SCXRD. However, in the case $CIGS_4$ and $CIGS_6$ (see Figure S2 in S.I), extra phases had to be considered to explain all reflections. Indeed, these secondary phases can be considered as polytypes since EDX analyses confirm a single chemical composition and electron diffraction attest to the existence of at least two kinds of crystals. Refined cell parameters and EDX results are all summarized in Table 3. Four polytypes have been identified for $CIGS_4$ and two for $CIGS_6$.

Table 3. Cell parameters of $CIGS_4$, $CIGS_5$ and $CIGS_6$ issued from a Le Bail refinement of the collected XRD pattern and chemical compositions issued from a EDX analysis.

	S G	a(Å)	c(Å)	EDX composition

$CIGS_4$	P-3*m*1	3.8246(2)	12.374(4)	
	R-3*m*	3.8256(1)	36.608(2)	$Cu_{0.32}In_{1.72}Ga_{0.84}S_4$
	P-3*m*1	3.8135(2)	30.737(3)	
	P-3*m*1	3.8100(4)	54.620(7)	
$CIGS_5$	P63*mc*	3.7979(1)	30.722(2)	$Cu_{0.63}In_{1.75}Ga_{1.38}S_5$
$CIGS_6$	P-3*m*1	3.8538(1)	18.6966(9)	
	P3*m*1	3.8510(3)	49.484(9)	$Cu_{1.14}In_{2.85}Ga_{0.63}S_6$

The existence of polytypes for the different members of the $((Cu,In,Ga)_{(Td)})_{n-2}(In_{(Oh)})S_n$ series is not surprising as exemplified for $ZnIn_2S_4$ that exhibits at least four polymorphs (i.e. $ZnIn_2S_4$ (I), $ZnIn_2S_4$(IIa), $ZnIn_2S_4$(IIb) and $ZnIn_2S_4$(IIIa)) that differs in the long rang ordering of the Td-Oh-Td blocks along the stacking axis and/or distribution of cations within Td sites. In fact, this propensity for polymorphism is observed for different members of the $Zn_mIn_2S_{3+m}$ series as discussed by H. Haeuseler et al [12]

Attempts to separate the two polymorphic forms of $CGIS_4$ and $CIGS_6$ via sulfurization of oxides was initiated and turn out to be successful for the latter. Indeed, as shown in Figure 6, the majority of experimental reflections observed in the PXRD could be indexed successfully by considering a single polymorph (SG *P-3m1* *a*=3.86, *c*= 18.69 Å).

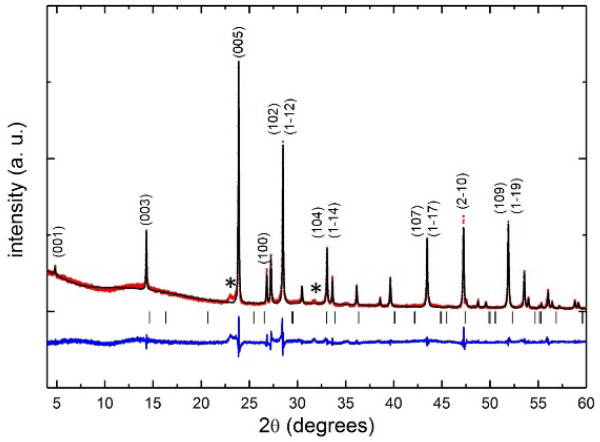

Figure 6. XRD pattern and Le Bail refinement of monophasic-CIGS6 compound Broad reflections (*) are slab intergrowths fingerprint.

Clearly, the driving force to the formation of lamellar $CIGS_n$ phases lies in the preference of In^{3+} cations for an octahedral environment in sulfides (even if In^{3+} cations can also be tetracoordinated), while Cu^+ and Ga^{3+} cations favor tetrahedral sites. Thus, all indium-free CGS ternary compounds existing in the $CuGaS_2$-Ga_2S_3 composition line (see Figure 1), exhibit structure types built upon the packing of $[MS_4]$ tetrahedra (i.e. chalcopyrite, stannite, or defect sphalerite). Tetrahedral coordination is always preferred independently the copper rate in the compound. In contrast, for gallium-free CIS compounds ($CuInS_2$-In_2S_3 line, a tiny copper vacancies rate is enough to destabilize the chalcopyrite structure of $CuInS_2$ (2Td sites) because the difference in site preference between copper and indium atoms. Thus, several compounds (i.e. $CuIn_5S_8$) with a spinel structure containing a majority of octahedral sites (1Td, 2 Oh) are formed.

The behavior of the CIGS quaternary compounds described in the composition zone $Cu_{1-z}Ga_{1+z/3}S_2$- $Cu_{1-z}In_{1+z/3}S_2$ (see Figure 1) is intermediate between that of thiogallates CGS and thioindates CIS, given the coexistence of gallium and indium in these compounds. As in the case of thioindates, copper vacancies rapidly destabilize the chalocopyrite structure and thus the tetrahedral environment of indium atoms. However, the presence of gallium seems to guide the structural evolution towards lamellar structures, in which the Td and Oh environments coexist even if, contrary to the spinel structure, tetrahedral coordination remains predominant: $CIGS_4$ (2Td, 1Oh), $CIGS_5$ (3Td, 1Oh), $CIGS_6$ (4Td, 1Oh) et $CIGS_7$ (5Td, 1Oh).

The flexibility of stoichiometric CIGS compounds to accept copper deficiencies as well as the identification of lamellar CIGS phases could be a key point to better understand structural phenomena described in the literature for CIGS-based solar cells. As a matter of fact, an angular step ($26° \leq 2\theta \leq 28°$) with asymmetric profile is observed in the PXRD patterns of Cu-poor CIGS thin films. This feature has been related to stacking faults occurrence in the bulk [16,17]. In Figure 7, the PXDR patterns of two CIGS thin films prepared by coevaporation, with experimental compositions $Cu_{0.89}In_{0.76}Ga_{0.24}S_2$ (Cu-poor) and $CuIn_{0.7}Ga_{0.3}S_2$ (Cu-stoichiometric) are compared to those of $CIGS_5$ and $CIGS_6$ compounds. As observed, some main reflections of lamellar compounds match fairly well with the broad angular step observed into the Cu-poor thin film pattern. This prompt us to wonder whether the stacking faults reported in the literature could actually correspond to the stabilization of the Cu-poor lamellar compounds. Actually, to deposit the CIGS absorber of a thin film solar cell, a multi-steps process is used including a Cu-poor stage. This last could facilitate the formation of lamellar compounds as secondary phases embedded into the chalcopyrite bulk. It is therefore important, to evaluate whether the optoelectronic properties of the lamellar $CIGS_n$ phases are very different from those of CIGS absorbers.

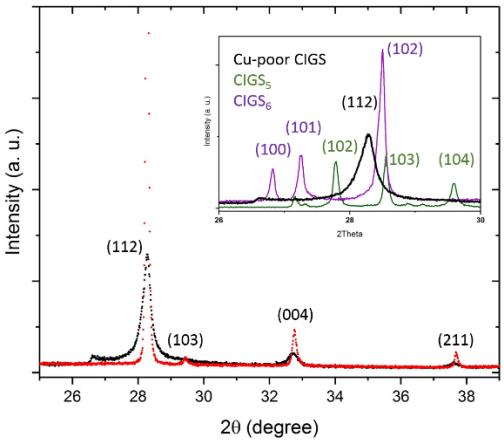

Figure 7. Comparison in the 25-39° 2θ-range of PXDR patterns of two CIGS thin films with experimental compositions Cu-poor $Cu_{0.89}In_{0.76}Ga_{0.24}S_2$ (black) and Cu-stoichiometric $CuIn_{0.7}Ga_{0.3}S_2$ (red). In the insert, the diagrams of $CIGS_5$ and $CIGS_6$ compounds are superimposed on broad angular step observed into the Cu-poor thin film pattern around the (112) reflection.

Optoelectronic properties of the lamellar $CIGS_n$ phases were analyzed by diffuse reflectance and X-ray photoelectron spectroscopies.

The Kubelka-Munk transformed diffuse reflectance spectra of $CIGS_4$, $CIGS_5$ and $CIGS_6$ prepared by sulfurization are shown in Figure 8. The spectrum of the stoichiometric $CuIn_{0.7}Ga_{0.3}S_2$ CIGS chalcopyrite compound is given for comparison. As inferred from Table 4, the optical gaps of four compounds are the same order of magnitude, however Eg slightly increases with copper content decreasing. Thus, chalcopyrite $CuIn_{0.7}Ga_{0.3}S_2$ with a Cu/S ratio equal to 0.5, exhibits an Eg ~ 1.6 eV while that of $CIGS_4$ compound (Cu/S = 0.08) is equal to 1.9 eV. It should be noted that the Eg measured for $CIGS_4$, should correspond to an average of those of two polymorphs coexisting These results suggest that these lamellar phases could be potential substitutes to Cu-poor CIGS chalcopyrite phases for tandem solar cell applications.

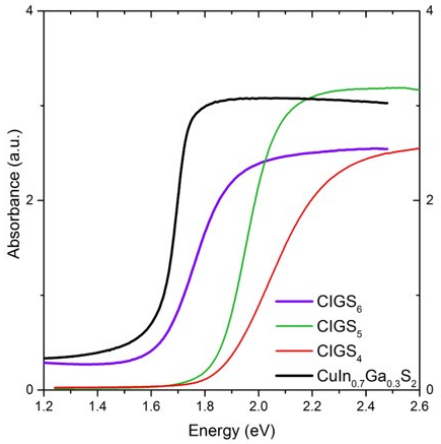

Figure 8. Kubelka-Munk transformed reflectance spectra of $CIGS_4$, $CIGS_5$, $CIGS_6$ and $CuIn_{0.7}Ga_{0.3}S_2$ chalcopyrite.

Table 4. Optical gaps and position of the uppermost level of the valence band vs. Fermi level

	Cu/S	E_g (eV)	VBM /E_F*
$CIGS_4$	0.08	1.9	1.0
$CIGS_5$	0.13	1.8	0.6
$CIGS_6$	0.2	1.6	0.9
$CIGS_7$	0.5	1.6	0.8

*The binding energy is referred to the E_F at BE=0 eV

XPS measurements were initiated to get insight on the nature of charge carriers and the positioning of the uppermost levels of the valence band. Spectra in the 0-10 eV binding energy range are plotted in Figure 9. The striking feature concerns the spectrum shape in the 0.5-6 eV domain, quite different for chalcopyrite and lamellar compounds. The former exhibits two well defined separated peaks the latter a unique broad band. At very first sight, based on the calculated electronic structures of $GaInS_3$ [18] the band peaking at ca. 4 eV might be associated with copper 3d orbitals hybridized with 3p orbitals of sulfur atoms, while the one at ca. 8 eV, much less intense, to Ga and In orbitals mixed with S.

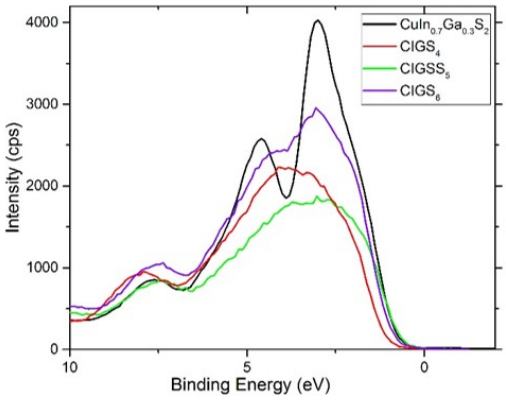

Figure 9. XPS valence band spectra of $CIGS_n$ series and $CuIn_{0.7}Ga_{0.3}S_2$ compound in [-10-0] eV range.

For the four investigated materials, the binding energy threshold is in the 0.5-1 eV range (Table 4). This suggests that $CIGS_4$, $CIGS_5$ and $CIGS_6$ materials are p-type semiconductors. More-

over, based on XPS and reflectance (absorption) measurements, the relative positions of valence and conduction bands of $CIGS_n$ compounds can be determined. An energy diagram is sketched in Figure 10. A slight change in the VB and CB positioning is noted. It may impact the electronic flow in a solar cell device and these materials would deserve to be tested as absorber.

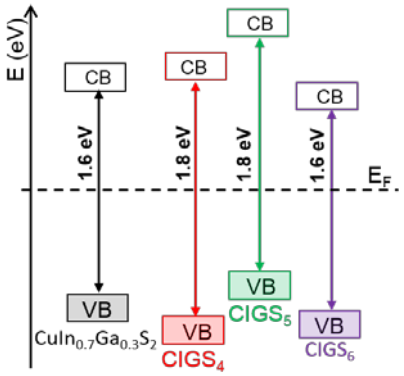

Figure 10. Sketch of the energy diagrams of probed materials

4.Concluding remarks

We reported here on the existence of several new lamellar $CIGS_n$ compounds in the $Cu_2S/In_2S_3/Ga_2S_3$ system. These materials built upon cations in 4-fold and 6-fold coordination of sulfur, exhibit a marked 2D character with a van der Waals gap what singularly contrasts with the 3D chalcopyrite $Cu(In,Ga)S_2$ materials with a dense structure consisting of only tetrahedra sharing edges. The aforementioned phases are very new members of the $(M(Td))_{n-2}In(Oh)S_n$ series that could be declined with In^{3+} cations in Oh environment and M^{m+} cations in Td environment. M^{m+} is a trivalent cation or a mixture of mono-, di- or trivalent cations, vacancies at the Td sites being possibly present to ensure the charge balance. Let us notice that In^{3+} cations in Oh site could be substituted for many other trivalent cations with a pronounced preference for the 6-fold coordination. Due the multiple possibilities to dispatch cations over tetrahedral sites with possible change in the long range ordering without modification of the overall stoichiometry, due to the strong similarities between all the building entities of the series, these materials are subject to stacking faults but also polytypisms and chemical composition deviations that open an avenue for the stabilization of new materials. Therefore, we are currently studying composition ranges for each $CIGS_n$ compound, by preserving their characteristic Cu/S and $Cu/In_{(Oh)}$ ratios but varying the $Ga_{(Td)}/In_{(Td)}$ one.

Surprisingly, optical gaps of $CIGS_4$, $CIGS_5$ and $CIGS_6$ compounds are comparable to the one of $Cu(In_{0.7}Ga_{0.3})S_2$ material currently investigated for potential use as absorber in tandem solar cell. This suggests this new series of materials may also present interesting characteristics for photovoltaic applications. Investigations are currently in progress to deposit them as thin films. Moreover, the very large range of possible compositions with multiples possible defects opens up the door to compounds with defect (intermediate) levels in the gap that can be benefit for photovoltaics but also for photocatalysis. These phases are currently explored to deepen our knowledge in these domains.

ASSOCIATED CONTENT

Supporting Information. (1) Typical PXRD patterns corresponding to nominal compositions $Cu_{0.7}(In_{0.7}Ga_{03})_{1.1}S_2$ (z=0.3, x=0.3), $Cu_{0.4}(In_{0.7}Ga_{0.3})_{1.2}S_2$ (z=0.6, x=0.3) and $Cu_{0.4}(In_{0.5}Ga_{0.5})_{1.2}S_2$ (z=0.6, x=0.5)., (2-5) Atom coordinates, ADP and occupancy rate of each atomic sites of $CIGS_4$, $CIGS_5$, $CIGS_6$, $CIGS_7$ respectively, (6) Interatomic distances for $CIGS_n$ compounds, (7-8) Atom coordinates, ADP and occupancy rate of each atomic sites of CIGS6 from PEDT data, (9) HAADF-STEM image of a faulted crystal, highlighting the propensity of CIGSn materials to contain intergrowth defects (10) PXRD patterns of as-prepared CIGS4 and CIGS6 compounds.

AUTHOR INFORMATION

Corresponding Author

* E-mail: maite.caldes@cnrs-imn.fr, catherine.deudon@cnrs-imn.fr.

AKNOWLEDGEMENTS

The authors acknowledge financial support from the CNRS-CEA "METSA" French network (FR CNRS 3507) on the plateform IRMA (CRISMAT – Caen).

REFERENCES

(1) Caballero, R.; Kaufmann, C. A.; Efimova, V.; Rissom, T.; Hoffmann, V.; Schock, H. W. Investigation of Cu(In,Ga)Se ₂ Thin-Film Formation during the Multi-Stage Co-Evaporation Process: CIGSe Thin-Film Formation Multi-Stage Co-Evaporation Process. *Prog. Photovolt. Res. Appl.* **2013**, *21* (1), 30–46. https://doi.org/10.1002/pip.1233.

(2) Thomere, A.; Guillot-Deudon, C.; Caldes, M. T.; Bodeux, R.; Barreau, N.; Jobic, S.; Lafond, A. Chemical Crystallographic Investigation on Cu2S-In2S3-Ga2S3 Ternary System. *Thin Solid Films* **2018**, *665*, 46–50. https://doi.org/10.1016/j.tsf.2018.09.003.

(3) Petricek V.; Dusek M. and Palatinus L. . The Crystallographic Computing System.

(4) Palatinus, L. *PETS-Program for Analysis of Electron Diffraction Data*; Institute of Physics of the CAS: Praha Czechia, 2011.

(5) Neal Fairley. *CasaXPS Software Ltd*.

(6) Kubelka, P.; Munk, F. An Article on Optics of Paint Layers. *Tech Phys* **1931**, *12*, 593–601.

(7) Amiraslanov, I.R; Azizov, T. Kh.; Guseinov, G.G.; Kuliev, A.S.; Niftiev, G.M. Crystal Growth, Structure, and Photoelectric Properties of New Polymorph of Gallium Indium Sulfide (GaInS3). *Izv. Akad. Nauk SSSR Neorganicheskie Mater.* **1988**, *24* (5), 723–726.

(8) Amiraslanov, I.R; Veliyev, R.B.; Misayev, A.A.; Asadov, S.G.; Gyseynov, G.G. On the Phase Formation in Ga2S-In2S3 System and the Crystal Structure of Ga0.5In1.5S3. *Doklady - Akademiya Nauk Azerbaidzhanskoi SSR*. 1990, pp 33–36.

(9) Amiraslanov, I.R; Asadov, F. Yu.; Musaev, A.A.; Guseinov, G.G. Crystal Structure of the New Layered Semiconductor Ga1.74In2.92S7. *Kristallografiya* **1989**, *34* (4), 1012–1013.
(10) Binsma, J. J. M.; Giling, L. J.; Bloem, J. PHASE RELATIONS IN THE SYSTEM Cu2 S—In2S3. *J. Cryst. Growth* **1980**, *50*, 429–436.
(11) Maeda, T.; Yu, Y.; Chen, Q.; Ueda, K.; Wada, T. Crystallographic and Optical Properties and Band Diagrams of $CuGaS_2$ and $CuGa_5S_8$ Phases in Cu-Poor Cu_2S–Ga_2S_3 Pseudo-Binary System. *Jpn. J. Appl. Phys.* **2017**, *56* (4S), 04CS12. https://doi.org/10.7567/JJAP.56.04CS12.
(12) Paorici, C.; Zanotti, L.; Gastaldi, L. Preparation and Structure of the CuIn5S8 Single-Crystalline Phase. *Mater. Res. Bull.* **1979**, *14* (4), 469–472. https://doi.org/10.1016/0025-5408(79)90187-9.
(13) Haeuseler, H.; Srivastava, S. K. Phase Equilibria and Layered Phases in the Systems A2X3±±M2X3±±MHX (A = Ga, In; M = Trivalent Metal; MH = Divalent Metal; X = S, Se). **1999**, 17.
(14) Ivashchenko, I. A.; Danyliuk, I. V.; Olekseyuk, I. D.; Pankevych, V. Z.; Halyan, V. V. Phase Equilibria in the Quasiternary System Ag2S–Ga2S3–In2S3 and Optical Properties of (Ga55In45)2S300, (Ga54.59In44.66Er0.75)2S300 Single Crystals. *J. Solid State Chem.* **2015**, *227*, 255–264. https://doi.org/10.1016/j.jssc.2015.04.006.
(15) Palatinus, L.; Corrêa, C. A.; Steciuk, G.; Jacob, D.; Roussel, P.; Boullay, P.; Klementová, M.; Gemmi, M.; Kopeček, J.; Domeneghetti, M. C.; et al. Structure Refinement Using Precession Electron Diffraction Tomography and Dynamical Diffraction: Tests on Experimental Data. *Acta Crystallogr. Sect. B Struct. Sci. Cryst. Eng. Mater.* **2015**, *71* (6), 740–751. https://doi.org/10.1107/S2052520615017023.
(16) Guo, Q.; Kim, S. J.; Kar, M.; Shafarman, W. N.; Birkmire, R. W.; Stach, E. A.; Agrawal, R.; Hillhouse, H. W. Development of $CuInSe_2$ Nanocrystal and Nanoring Inks for Low-Cost Solar Cells. *Nano Lett.* **2008**, *8* (9), 2982–2987. https://doi.org/10.1021/nl802042g.
(17) Rodriguez-Alvarez, H.; Barreau, N.; Kaufmann, C. A.; Weber, A.; Klaus, M.; Painchaud, T.; Schock, H.-W.; Mainz, R. Recrystallization of Cu(In,Ga)Se2 Thin Films Studied by X-Ray Diffraction. *Acta Mater.* **2013**, *61* (12), 4347–4353. https://doi.org/10.1016/j.actamat.2013.04.006.
(18) Khyzhun, O. Y.; Halyan, V. V.; Danyliuk, I. V.; Ivashchenko, I. A. Electronic Structure of (Ga55In45)2S300 and (Ga54.59In44.66Er0.75)2S300 Single Crystals. *J. Mater. Sci. Mater. Electron.* **2016**, *27* (4), 3258–3264. https://doi.org/10.1007/s10854-015-4153-2.

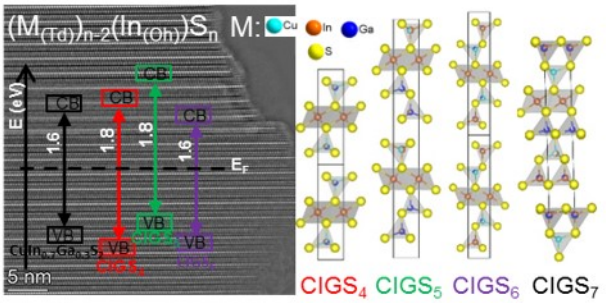

Several new layered materials, $CIGS_n$ have been evidenced in the Cu_2S-In_2S_3-Ga_2S_3 system. $(M(Td))_{n-2}(In(Oh))S_n$ slabs are separated from each other by a van der Waals gap and subscript n refers to the number of sulfur layers within the building block. Their optical gap is quite similar to the one of the $Cu(In_{0.7}Ga_{0.3})S_2$ chalcopyrite absorbers used in tandem solar cells. They might be very attractive for photovoltaic applications in thin film devices but also for photocatalysis.

Supporting Information for "New layered quaternary compounds in the Cu_2S-In_2S_3-Ga_2S_3 system"

M.T. Caldes*, C. Guillot-Deudon*, A. Thomere, M. Penicaud, Eric Gautron, P. Boullay†, M. Bujoli-Doeuff, Nicolas Barreau, S.Jobic, A. Lafond

Institut des Matériaux Jean Rouxel – Université de Nantes, CNRS, 2 rue de la Houssinière, BP 32229, 44322 Nantes Cedex 3, France

†CRISMAT, CNRS, Normandie University, ENSICAEN, UNICAEN, 14000 Caen, France

Corresponding Authors

* E-mail: maite.caldes@cnrs-imn.fr, catherine.deudon@cnrs-imn.fr.

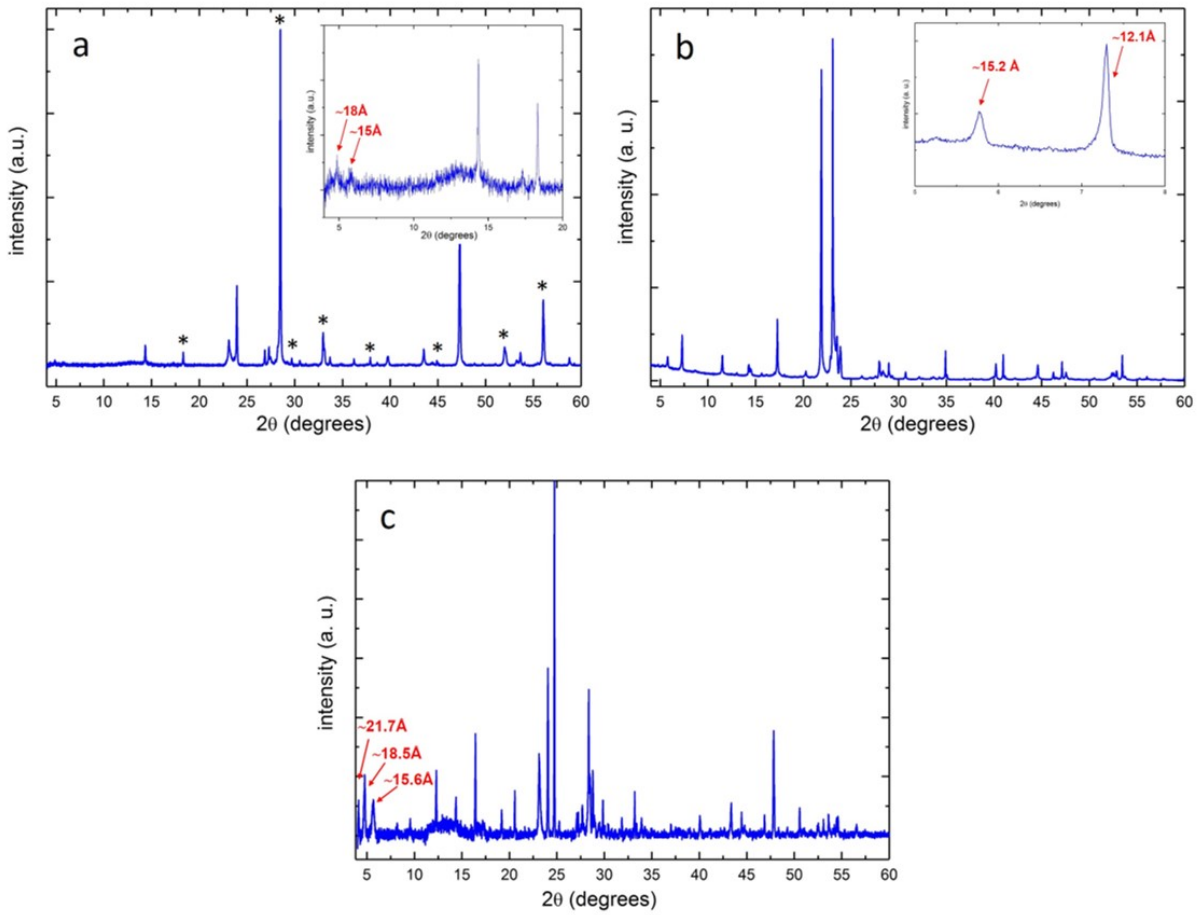

Figure S1: Typical PXRD patterns corresponding to nominal compositions: (a) $Cu_{0.7}(In_{0.7}Ga_{03})_{1.1}S_2$ (z=0.3, x=0.3), (b) $Cu_{0.4}(In_{0.7}Ga_{0.3})_{1.2}S_2$ (z=0.6, x=0.3) and (c) $Cu_{0.4}(In_{0.5}Ga_{0.5})_{1.2}S_2$ (z=0.6, x=0.5). In Figure S1a, the reflections corresponding to a chalcopyrite-type compound are asterisk marked.

Table S1. Synthesis conditions of all the targeted compositions

Targeted composition	T(°C)	Rate(°/h)	Temps(h)	Cooling rate(°/h	precursors
$Cu_{0.4}(In_{0.5}Ga_{0.5})_{1.2}S_2$	850	100	340*	100	Cu, In, Ga,S
$Cu_{0.7}(In_{0.7}Ga_{0.3})_{1.1}S_2$	850	100	340*	100	Cu, In, Ga,S
$Cu_{0.4}(In_{0.7}Ga_{0.3})_{1.2}S_2$	850	100	170h	100	Cu, In, Ga,S
$CIGS_4$	850	100	48	quenched	Cu_2S, In_2S_3, Ga2S3
$CIGS_5$	850	100	48	quenched	Cu_2S, In_2S_3, Ga2S3
$CIGS_6$	850	100	48	quenched	Cu_2S, In_2S_3, Ga2S3
$CIGS_6$ (sulfurization)	900	300	3	100	Cu_2O, In_2O_3,Ga_2O_3 H2S

*With intermediate reheating steps

Table S2. Atom coordinates, isotropic atomic displacement parameters, and occupancy rate of each atomic sites of CIGS4

	s.o.f.	x	y	z	U_{eq}(Å²)
In1	1	0	0	0.5	0.0204(2)
Cu2	0.16	2/3	1/3	0.1893(2)	0.0257(7)
In2	0.37	-	-	-	-
Ga2	0.42	-	-	-	-
S1	1	2/3	1/3	0.3849(4)	0.0138(9)
S2	1	1/3	2/3	0.1247(4)	0.024(1)

Table S3. Atom coordinates, isotropic atomic displacement parameters, and occupancy rate of each atomic sites of CIGS5

	s.o.f.	x	y	z	U_{eq}(Å²)
In1	1	0	0	0.33037(5)	0.0201(2)
Ga1	0.7	2/3	-1/3	0.11072(5)	0.0203(3)
In_Ga1	0.3	-	-	-	-
Ga2	0.7002	1/3	-1/3	0.20969(6)	0.0170(5)
Cu_Ga2	0.0974	-	-	-	-
In3	0.4467	-1/3	1/3	0.45459(5)	0.0221(3)
Cu_In3	0.5533	-	-	-	-
S1	1	-1/3	1/3	0.3769(2)	0.0134(7)
S2	1	1/3	-1/3	0.2848(2)	0.0146(6)
S3	1	-2/3	2/3	0.4812(2)	0.0256(11)
S4	1	1/3	-1/3	0.0821(2)	0.0238(9)
S5	1	2/3	-2/3	0.1867(2)	0.0196(10)

Table S4. Atom coordinates, isotropic atomic displacement parameters, and occupancy rate of each atomic sites of CIGS6

	s.o.f.	x	y	z	U_{eq}(Å²)
In1	1	0	0	0.5	0.0165(5)
Cu1	0.72	1/3	2/3	0.29990(10)	0.0118(5)
Ga1	0.28	-	-	-	-
In2	0.8836	1/3	2/3	0.87059(9)	0.0233(5)
Ga2	0.1	-	-	-	-
S1	1	1/3	2/3	0.4260(2)	0.0102(7)
S2	1	1/3	2/3	0.7420(2)	0.0169(10)
S3	1	1/3	2/3	0.0808(3)	0.0214(11)

Table S5. Atom coordinates, isotropic atomic displacement parameters, and occupancy rate of each atomic sites of CIGS7

	s.o.f.	x	y	z	U_{eq}(Å²)
In1	1	1/3	2/3	0.6644(4)	0.0205(12)
In2	0.2888	0	0	0.9815(2)	0.012(2)
Ga2	0.7112	-	-	-	-
In3	0.7682	-2/3	2/3	0.2056(3)	0.031(2)
Ga3	0.2318	-	-	-	-
Ga4	0.857	0	0	0.4919(3)	0.008(2)
Cu5	0.1	-1/3	1/3	0.3501(5)	0.025(3)
Ga5	0.4333	-	-	-	-
Cu6	1	2/3	1/3	0.8377(4)	0.019(2)
S1	1	0	0	0.5998(8)	0.017(4)
S2	1	-1/3	1/3	0.4644(14)	0.045(9)
S3	1	1/3	-1/3	0.0205(6)	0.016(4)
S4	1	-2/3	2/3	0.3155(12)	0.042(8)
S5	1	2/3	1/3	0.7310(6)	0.010(4)
S6	1	0	0	0.8740(5)	0.003(3)
S7	1	0	0	0.1640(10)	0.042(5)

Table S6. Interatomic distances for $CIGS_4$, $CIGS_5$, $CIGS_6$ $CIGS_7$. compounds, compared to those reported in the literature for other phases with similar chemical environments

	In-S (Å)	Ga-S/Cu-S	(Ga,□)-S (Cu,□)-S (Ga,Cu,□)-S	(Cu,In)-S (Ga,In)-S	(Cu,In,□)-S (Ga,In,□)-S
$GaInS_3$ [6]	2.61		2.30		2.32-2.39
$CuIn_5S_8$[11]	2.59-2.62			2.41-2.46	
$CuInS_2$[10]	2.42				
$CuGaS_2$[11]		2.37			
Cu-poor $CuGaS_2$[2]		2.30	2.24-2.26		
Cu-poor $Ag_{1.25}Ga_{2.5}In_{3.75}S_{10}$[13]	2.60-2.64			2.36-2.41	2.31-2.39
$CIGS_4$	2.61				2.33-2.39
$CIGS_5$	2.60		2.30	2.33-2.39	
$CIGS_6$	2.62	2.36			2.40
$CIGS_7$	2.59	2.30-2.33	2.27-2.32	2.37	2.31-2.46

Table S7. Main crystal data and structure PEDT refinement results for $Cu_{1.2}In_{2.54}Ga_{1.06}S_6$ ($CIGS_6$ structure-type)

	CIGS6-PEDT
a (Å) (2)	3.8974
c (Å) (2)	18.4267
Space Group	P-3*m*1
# refined param.	90
N_{obs}/N_{all} (unique)	2755/6825
R(obs/all)	18.47/25.31
R_w(obs/all)	39.21/39.21
ρ (e^-/Å³)+/-	1.76/-0.53

Table S8. Atom coordinates, isotropic atomic displacement parameters, and occupancy rate of each atomic sites of CIGS6 from PEDT data

	s.o.f.	x	y	z	U_{eq}(Å²)
In1	1	0	0	0.5	0.04917(1)
Cu1	0.6	2/3	1/3	0.3008	0.02539(1)
Ga1	0.4	-	-	-	-
In2	0.7672	2/3	1/3	0.872(9)	0.03972(5)
Ga2	0.1332	-	-	-	-
S1	1	2/3	1/3	0.4269(2)	0.03232(7)
S2	1	2/3	1/3	0.7408(2)	0.02433(10)
S3	1	2/3	1/3	0.0809(3)	0.0407(11)

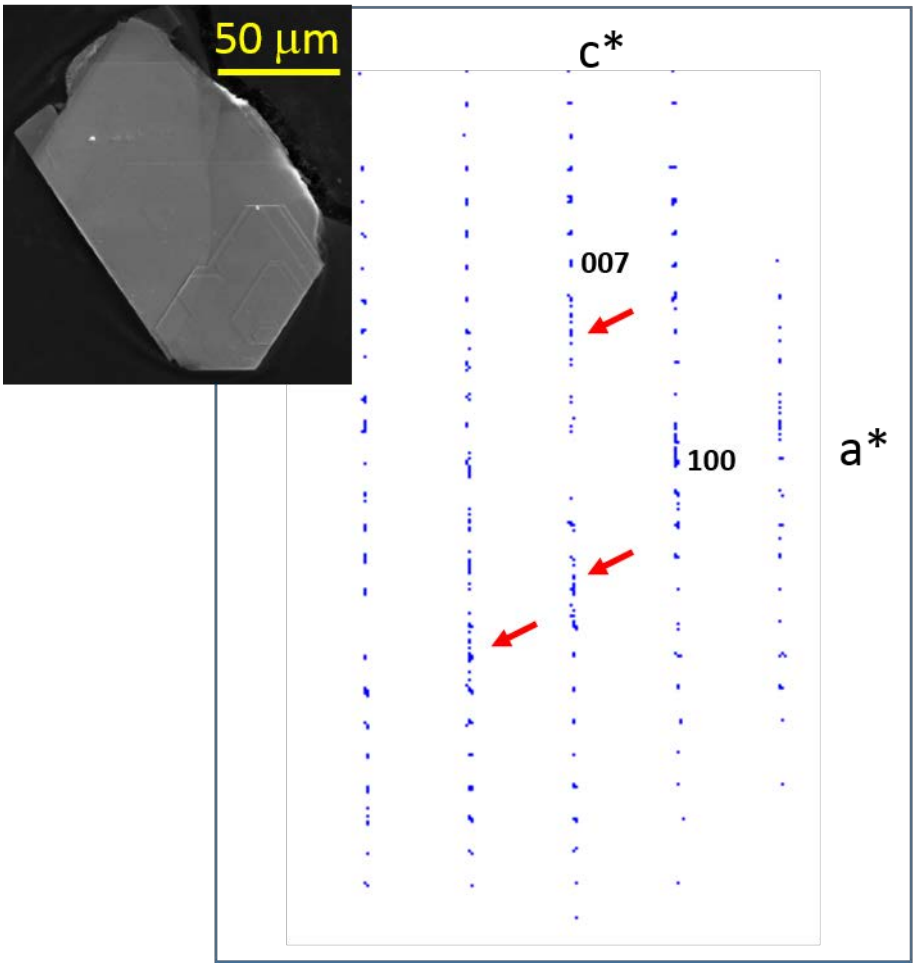

Figure S2 HA

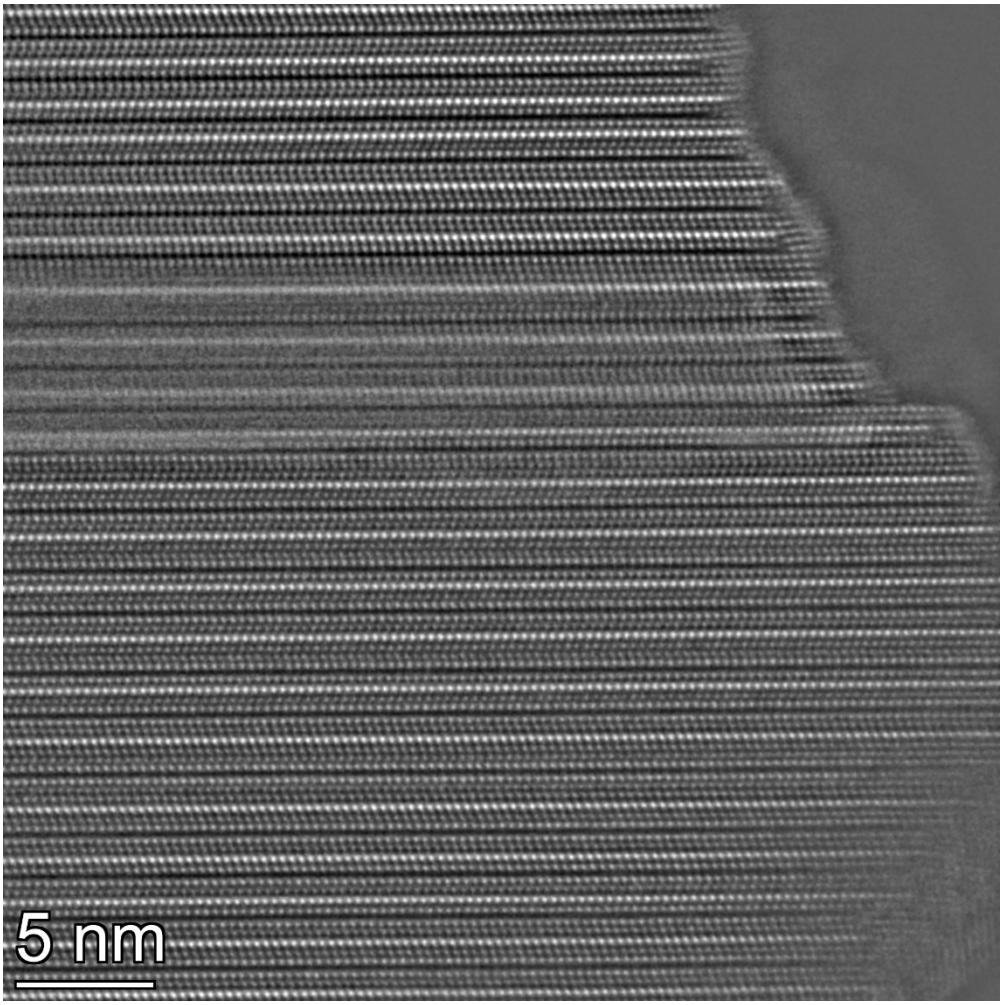

Figure S3. HAADF-STEM image of a faulted crystal, highlighting the propensity of CIGSn materials to contain intergrowth defects.

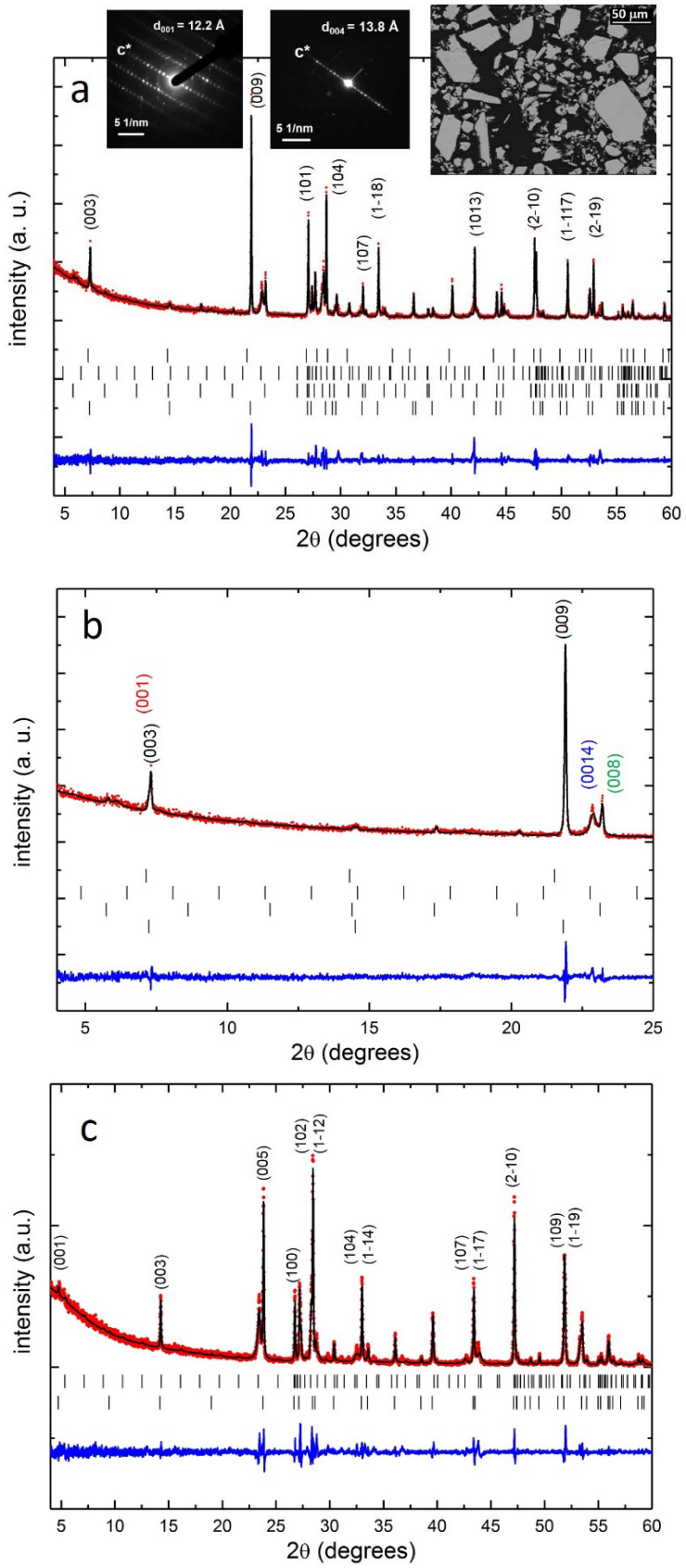

Figure S4. PXRD patterns of as-prepared: (a-b) $CIGS_4$ and (c) CIGS6 compounds. The homogeneous contrast observed in the backscattered electron image confirm a single chemical composition while electron diffraction patterns attest to the existence of at least two kinds of crystals. The enlargement of $CIGS_4$ pattern between 4-25° (see picture b) shows one (ool) reflection indexed for each polytype (different colors)

Targeted composition	T(°C)	Rate(°/h)	Temps(h)	Cooling rate(°/h	precursors
$Cu_{0.4}(In_{0.5}Ga_{0.5})_{1.2}S_2$	850	100	340*	100	Cu, In, Ga,S
$Cu_{0.7}(In_{0.7}Ga_{0.3})_{1.1}S_2$	850	100	340*	100	Cu, In, Ga,S
$Cu_{0.4}(In_{0.7}Ga_{0.3})_{1.2}S_2$	850	100	170h	100	Cu, In, Ga,S
$CIGS_4$	850	100	48	quenched	Cu_2S, In_2S_3, Ga2S3
$CIGS_5$	850	100	48	quenched	Cu_2S, In_2S_3, Ga2S3
$CIGS_6$	850	100	48	quenched	Cu_2S, In_2S_3, Ga2S3
$CIGS_6$ (sulfurization)	900	300	3	100	Cu_2O, In_2O_3,Ga_2O_3 H2S

*With intermediate reheating steps